Volume 1 | Number 1 | Jan 2013 | Pages 1–100

Journal of
Materials Chemistry A

Materials for energy and sustainability
www.rsc.org/materialsA

ROYAL SOCIETY OF CHEMISTRY

ROYAL SOCIETY OF CHEMISTRY

www.rsc.org/materialsA

Theory of Mass Transport in Sodium Alanate

Kyle Jay Michel and Vidvuds Ozoliņš[*]

Sodium alanate, NaAlH$_4$, is a well-known hydrogen storage material that decomposes into Na$_3$AlH$_6$ and Al while releasing H$_2$ as a gas. While the thermodynamics of this reaction are ideal for applications in fuel cell vehicles, the reaction rates are prohibitively slow unless the material is doped with transition metals (such as titanium) or rare earths (such as cerium). It has been widely theorized that the flux of point defects through the bulk phases provides the mechanism for long-range metal transport which accompanies the hydrogen release and absorption reactions. In this paper, a quantitative model is introduced to describe mass transport using point defect energies obtained from first-principles density-functional theory (DFT) calculations. It is found that negatively charged sodium vacancies in Na$_3$AlH$_6$ have the largest flux of all metal-site defects in any of the phases, at all temperatures examined. Positively charged hydrogen vacancies are predicted to balance the charge of sodium vacancies and have a higher diffusivity than this metal defect. The activation energy for the formation and diffusion of sodium vacancies in Na$_3$AlH$_6$ is found to be equal to 50 kJ/mol for rehydrogenation and 70 kJ/mol for dehydrogenation, in good agreement with experimental values. It is argued that diffusion of sodium vacancies in Na$_3$AlH$_6$ represents the rate-limiting process in the dehydrogenation of Ti-doped NaAlH$_4$ and that Ti must catalyze some other process (or processes) than bulk mass transport.

1 Introduction

In the search for a hydrogen storage material that meets all of the requirements for applications in fuel cell vehicles,[1,2] sodium alanate, NaAlH$_4$, has been the focus of a considerable amount of research (a selected list of publications includes Refs.[3–11]). This prototypical complex metal hydride undergoes a multi-step dehydrogenation reaction for which the first steps follow[12,13]

$$\text{NaAlH}_4 \rightarrow \frac{1}{3}\text{Na}_3\text{AlH}_6 + \frac{2}{3}\text{Al} + \text{H}_2, \qquad (1)$$

$$\text{Na}_3\text{AlH}_6 \rightarrow 3\text{NaH} + \text{Al} + \frac{3}{2}\text{H}_2. \qquad (2)$$
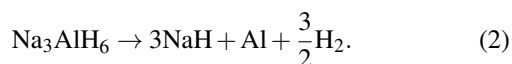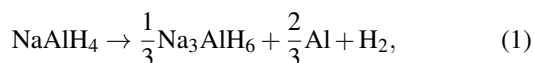
The equilibrium temperatures for Reactions (1) and (2) at an H$_2$ pressure of 1 bar are 33 and 110 °C, respectively, although they are limited by prohibitively slow kinetics at temperatures even well above these.[6] In a landmark discovery, Bogdanovic and Schwickardi[3] found that doping with small concentrations of Ti significantly increased the reaction rates. The uncatalyzed activation energy for Reaction (1) was found to be equal to 118 kJ/mol and, upon Ti doping, this is reduced to between 73 and 80 kJ/mol in the catalyzed reaction, with the rate constant increasing with Ti content.[7,14] Similarly, the activation energy for Reaction (2) is reduced from 120 kJ/mol to 97 kJ/mol upon doping with Ti.[7,14] Additionally, the reactions

are made reversible under conditions that could be achieved in fuel cell vehicles[3,6,14] with catalyzed activation energies for rehydrogenation equal to 62 and 56 kJ/mol for Reactions (1) and (2), respectively.[14]

A primary focus of the experimental and theoretical work on NaAlH$_4$ has been on identifying the atomic level processes involved in the de- and rehydrogenation reactions and how these processes are catalyzed by Ti. Although Reactions (1) and (2) do not meet the gravimetric storage requirements for vehicular applications, an understanding of this catalytic effect will aid in the improvement of other reactions involving complex metal hydrides that have desirable thermodynamic properties[15–28] but which are limited by slow kinetics. Both metal and hydrogen diffusion have received significant attention as they are obvious candidates in the search for rate-limiting kinetic mechanisms. For instance, experimental studies have suggested that long-range bulk diffusion likely represents the rate-limiting process of Reaction (1) when doped with Ti.[29] Additionally, hydrogen-deuterium exchange experiments show that it is likely a metal-site defect (i.e. not a pure hydrogen defect) that is the rate-limiting diffusive species.[9,10]

First-principles calculations are well-suited to the task of exploring atomic level processes in Reactions (1) and (2) and have been applied in past work.[30–39] However, a full quantitative treatment of mass transport during a solid-state reaction is difficult due to the many possible pathways along which a reaction may proceed. As a result, a general agreement between experimental and computational work on rate-limiting processes in Reaction (1) (in either pure or doped systems) does

Department of Materials Science and Engineering, University of California, Los Angeles, P.O. Box 951595, Los Angeles, California 90095-1595
E-mail: vidvuds@ucla.edu

not exist. In this paper we develop a framework to study mass transport by connecting first-principles density-functional theory (DFT) calculations of point defect properties in crystals to the macroscopic evolution of a reaction. This allows us to identify the fastest modes of mass transport during Reactions (1) and (2) and to calculate the corresponding activation energies. The methods described in this paper are applicable to general solid-state decomposition reactions and diffusion-driven phase transformations.

This work is the final paper is a series by these same authors in which the equilibrium concentrations of native defects,[40] their diffusivities,[41] and the effects of Ti substitutions on the native defect concentrations[42] have all been examined. The results of these papers are combined in a model to describe the flux of defects through the phases of Reaction (1). In the past, studies of point defect energetics and diffusivities have focused only on defects in $NaAlH_4$. We expand this by considering defects in all of the phases involved in the reaction in order to identify which is truly the dominant mechanism of mass transport. This paper discusses the connection between the morphology and temperature dependence of the reaction rates, as well as their relation to microscopic atomic-level quantities such as point defect formation and migration energies. We find that the fastest mass transport mechanism occurs via Na vacancies in Na_3AlH_6 (the charge of which is balanced by hydrogen vacancies), consistent with experimental work in which it was found that the largest concentrations of defects were in a product phase of Reaction (1).[43] We go on to argue that this is the rate-limiting process in the dehydrogenation of Ti-doped systems where the calculated activation energy (70 kJ/mol) and experimental activation energy for the overall reaction (73-80 kJ/mol[6]) are in good agreement.

2 Model and Methods

2.1 Reaction Morphologies

The spatial arrangement and physical contact between the reactant and product phases directly influence the diffusional fluxes that are involved in Reaction (1). Schematic one-dimensional (1D) model morphologies are shown in Figure 1(a)-(b) and have been discussed previously in Ref. 40. In addition to this discussion, we note the possibility of Mullins-Sekerka type[44] instabilities of the advancing planar reaction fronts. For instance, the Na_3AlH_6/Al interface in Figure 1(a) may become unstable with respect to a sinusoidal modulation, which is shown by a dashed line. This modulation increases the concentration gradients and fluxes at the protrusions to the left of the interface, leading to increased growth of the Al phase and amplification of the initial perturbation. The existence and critical wavelength for these instabilities are determined by multiple factors such as slow interfacial reac-
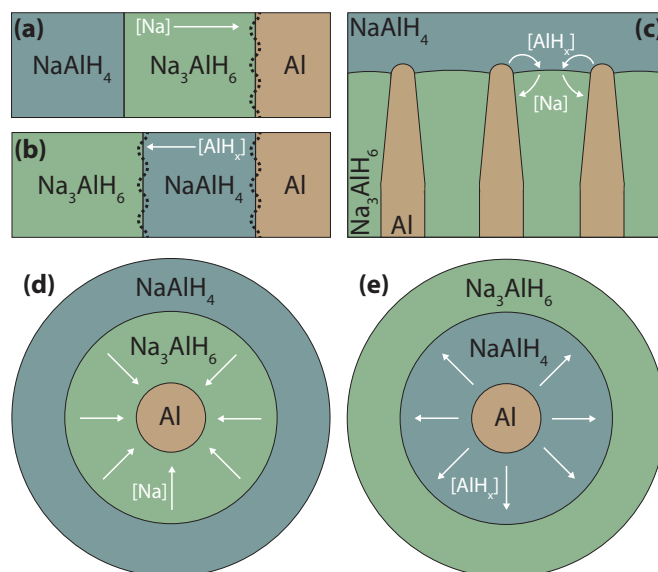
Fig. 1 Model morphologies used to study defect fluxes in Reaction (1).

tions and fast diffusion along the advancing interface, which both tend to stabilize the planar interface. If present, instabilities will lead to more complex reaction morphologies, such as those shown in Figure 1(c) and discussed below.

Here, we go beyond the simple 1D case and examine prototypical morphologies that are commonly encountered in eutectoid solid-state reactions. In all morphologies, we consider diffusion through $NaAlH_4$ and Na_3AlH_6, but not through Al. In Ref. 40 we showed that the concentrations of metal defects in Al are much lower than in either $NaAlH_4$ or Na_3AlH_6 and therefore cannot measurably contribute to metal segregation. It was also found that diffusion of negatively charged Na vacancies in Na_3AlH_6 and neutral AlH_3 and charged AlH_4 vacancies in $NaAlH_4$ are the prevalent metal mass transport mechanisms for Reaction (1).[40–42]

We first consider a lamellar morphology in which mass transport can occur simultaneously through both hydrides [Figure 1(c)]. Here, the relative thickness of the Al lamella increases with the distance from the reaction front until reaching the limiting ratio determined by the volume fractions of the products of Reaction (1). Na vacancy diffusion through the Na_3AlH_6 phase leads to an outward growth of Na_3AlH_6 and gradual widening of the Al lamella behind the reaction front. The second diffusion mechanism, Al-site vacancy diffusion through $NaAlH_4$, enables phase separation into Al-rich and Na-rich reaction products (Al and Na_3AlH_6, respectively) ahead of the forward-moving reaction front. For both mechanisms, the average diffusion length is determined by the inter-lamellar spacing which, once established, stays constant throughout the reaction. The relative diffusion rates of Al-site

vacancies in NaAlH$_4$ ($D_{[\text{AlH}_x]}$) and Na vacancies in Na$_3$AlH$_6$ ($D_{[\text{Na}]}$) determine the degree of tapering of the Al lamella. For instance, in the limiting case of rapid diffusion through the reactant, $D_{[\text{AlH}_x]} \gg D_{[\text{Na}]}$, the lamella become straight (untapered), while for $D_{[\text{AlH}_x]} \ll D_{[\text{Na}]}$, the tips of the Al lamella in contact with NaAlH$_4$ become very sharp and all mass transport occurs via Na vacancies through the Na$_3$AlH$_6$ phase. The reverse rehydrogenation reaction can occur by reversing the mass fluxes shown in Figure 1(c).

The second morphology describes the so-called expanding (or contracting) envelope morphology where all mass transport occurs through Na$_3$AlH$_6$ [Figure 1(d)]. Here, the initial nucleation of the reaction product phases is followed by a growth stage, which proceeds via Na vacancy diffusion from the NaAlH$_4$/Na$_3$AlH$_6$ interface towards the Na$_3$AlH$_6$/Al interface. The thickness of the expanding Na$_3$AlH$_6$ shell increases over time, with the diffusion distances and reaction rates being faster at the early stages of the reaction. Rehydrogenation may proceed either by reversing the diffusional fluxes in [Figure 1(d)] or by nucleating the NaAlH$_4$ phase between Al and Na$_3$AlH$_6$, establishing the morphology shown in Figure 1(e). In the latter case, diffusion of Al-site vacancies through NaAlH$_4$ provides the necessary mass transport mechanism. Figure 1(e) also represents a possible dehydrogenation morphology where the inner NaAlH$_4$ shell shrinks by growing the Al core and the outer Na$_3$AlH$_6$ shell.

2.2   Diffusional Fluxes

The drift-diffusion-reaction equation for the concentration of a point defect i, C_i, can be written as[45]

$$\frac{\partial C_i}{\partial t} = \nabla(D_i \nabla C_i) + \frac{q_i D_i}{k_B T} \nabla(C_i \nabla \varphi) - \sum_{j,k} K^{\text{dis}}(i \to j,k) C_i +$$
$$\sum_{j,k} K^{\text{rec}}(j,k \to i) C_j C_k, \tag{3}$$

where the term on the left side is its partial derivative with respect to time. In the first term on the right side (due to the Fickian flux), D_i is the diffusivity of defect i. In the second term (due to the drift flux under an electric field), q_i is the charge of the defect, k_B is the Boltzmann constant, T is the temperature, and φ is the electric potential, which can be determined by solving Poisson's equation

$$\nabla^2 \varphi = -\frac{\rho}{\varepsilon}, \tag{4}$$

where ρ is the charge density and ε is the dielectric permittivity. In the last two terms on the right side of Eq. (3), $K^{\text{dis}}(i \to j,k)$ and $K^{\text{rec}}(j,k \to i)$ represent, respectively, the rates of dissociation/recombination of defect i into/from defects j and k. Equations (3) and (4) need to be complemented

by appropriate morphology- and (implicitly) time-dependent boundary conditions for the potentials and concentrations. General treatment of these equations would lead to a highly complex system of nonlinear partial differential equations.

To simplify the problem, we assume local equilibrium between all defect concentrations so that the last two terms of Eq. (3) cancel. The electric field in these equations results from a separation of charged defects due to different diffusion rates, but requires an increase in the total free energy of the system due to the build-up of long-range polarization fields. Therefore, it is unlikely that a significant long-range separation of charge occurs, but instead local charge equilibria are established at all interphase boundaries, minimizing the electrostatic energy of the system. As a consequence, the charge density ρ and the potential φ are negligible so that the drift flux can be ignored. Finally, we find that the defect concentrations are very low and one can neglect any composition-dependence of the diffusivities D_i. With these simplifications, Eq. (3) reduces to

$$\frac{\partial C_i}{\partial t} = D_i \nabla^2 C_i. \tag{5}$$

In what follows, we discuss how morphology affects diffusional fluxes, reaction rates, and their apparent temperature dependence. In particular, we find solutions to Eq. (5) subject to conditions imposed by one-, two-, and three-dimensional morphologies shown in Figure 1. We do not treat charge transport explicitly since it was shown in Ref. 41 that for all charged metal defects (e.g., AlH$_4$ vacancies in NaAlH$_4$ or Na vacancies in Na$_3$AlH$_6$) compensating charge transport via hydrogen vacancies and/or hydrogen interstitials is much faster than metal diffusion. We also adopt the assumption used in Ref. 40 that the defect concentration profile $C_i(\mathbf{r},t)$ equilibrates at a rate that is much faster than the movement of the boundaries. Hence, we can neglect the $\partial C_i/\partial t$ term in the diffusion equation and solve the stationary problem:

$$D_i \nabla^2 C_i = 0, \tag{6}$$

subject to local equilibrium boundary conditions at the heterophase interfaces. The atomic-scale structure of the heterophase interfaces in Figure 1 and the interfacial kinetics of bond breaking and phase transformations may in reality be quite complex, but here we are only concerned that a local equilibrium exists between the phases present at a particular interface and that this equilibrium determines the chemical potentials of the atomic species involved in the reaction.[40] These assumptions naturally lead to the existence of defect concentration gradients whenever the temperature deviates from the critical temperature of Reaction (1) due to the fact that chemical potentials of Na and Al, and hence the metal-site defect concentrations at the heterophase interfaces in Figure 1, are different (see below).

2.3 Defect thermodynamics

The equilibrium concentration of a defect i (per site) in the dilute limit is

$$C_i = N_i e^{-\Delta G_i / k_B T} \qquad (7)$$

where k_B is the Boltzmann constant, T is the temperature, and N_i is the symmetry factor accounting for the entropy due to the number of equivalent ways that a defect can be introduced at a single site. The free energy of formation, ΔG_i, is equal to

$$\Delta G_i = \Delta G_i(\text{def}) - \sum_{s=1}^{N_{\text{species}}} n_s^i \mu_s + q_i(E_{\text{VBM}} + \varepsilon_F). \qquad (8)$$

Here, $\Delta G_i(\text{def})$ is the change in the total free energy of a crystal due to the introduction of a defect i. The sum in Eq. (8) runs over all elements where μ_s is the chemical potential of element s and n_s^i is the number of atoms of type s that were added ($n_s^i > 0$) or removed ($n_s^i < 0$) to create defect i. Finally, q_i is the charge of defect i and ε_F is the Fermi level referenced to the valence band maximum (VBM), E_{VBM}. The chemical potentials of the elements and electrons are discussed in the remainder of this section.

In all of the morphologies, charged defect concentrations must be compensating to preserve the overall charge neutrality of the system. In order to prevent the formation of long-range electric fields, a local charge neutrality was enforced in all calculations. Formally, this corresponds to the condition that

$$\sum_{i=1}^{N_{\text{defects}}} C_i q_i = 0 \qquad (9)$$

at each local environment where q_i is the charge of defect i and C_i is its concentration determined by Eq. (7). Solution of Eq. (9) determines the Fermi level that appears in Eq. (8); the latter is a function of the temperature, partial pressure of hydrogen gas, defect energies and the set of chemical potentials of the coexisting phases.

The concentration gradients that appear in the fluxes exist because the elemental chemical potentials and the Fermi energies for charged defects can differ between interfaces in Figure 1, which are manifested as different formation energies in Eq. (8). Although a local equilibrium exists at each interface, this describes a system that as a whole is out of equilibrium. The interfaces shown in Figure 1 determine the chemical potentials of the elements (the corresponding equations can be found in Ref. 40). Examining the 1D morphology in Figure 1(a) (although this exact discussion applies to the 2D and 3D morphologies as well), we label the chemical potential of element X at the interface between NaAlH$_4$ and Na$_3$AlH$_6$ as μ_X^L and at the interface between Na$_3$AlH$_6$ and Al as μ_X^R. It can be shown[40] that the differences in the chemical potentials be-

tween these interfaces are

$$\mu_{\text{Al}}^R - \mu_{\text{Al}}^L = \frac{3}{2}\Delta G_{\text{rxn}},$$
$$\mu_{\text{Na}}^R - \mu_{\text{Na}}^L = -\frac{1}{2}\Delta G_{\text{rxn}}, \qquad (10)$$

where ΔG_{rxn} is the change in free energy of Reaction (1) (*products - reactants*). Under dehydrogenation conditions, $\Delta G_{\text{rxn}} < 0$ so that $\mu_{\text{Al}}^L > \mu_{\text{Al}}^R$. This will result in a thermodynamic driving force for Al to the interface with solid Al (or Al vacancies in the opposite direction) so that this product phase is grown. Similarly, under these conditions $\mu_{\text{Na}}^L < \mu_{\text{Na}}^R$ so that the flux of Na is to the NaAlH$_4$ interface (or in the opposite direction for Na vacancies) so that the Na$_3$AlH$_6$ phase can grow to the left and NaAlH$_4$ is consumed. This same argument applies under rehydrogenation conditions during which $\Delta G_{\text{rxn}} > 0$. In this case, the directions of the chemical potential gradients are reversed so that Na$_3$AlH$_6$ and Al are consumed while NaAlH$_4$ is grown.

The morphology in Figure 1(b) corresponds to that in which the flux of defects is through NaAlH$_4$ and the chemical potentials at the left (L) and right (R) interfaces are respectively determined by equilibria with NaAlH$_4$ and Al. The chemical potential differences are here equal to

$$\mu_{\text{Al}}^L - \mu_{\text{Al}}^R = \frac{3}{2}\Delta G_{\text{rxn}},$$
$$\mu_{\text{Na}}^L - \mu_{\text{Na}}^R = -\frac{3}{2}\Delta G_{\text{rxn}}. \qquad (11)$$

Again, the gradients are such that NaAlH$_4$ is grown at low temperatures and consumed at high temperatures.

For a detailed discussion on the methods used to calculate all values discussed to this point, see Ref. 40. To summarize, we used density-functional theory (DFT) as implemented in the Vienna Ab-initio Simulation Package (VASP).[46] We used the generalized gradient approximation (GGA) to the exchange-correlation functional according to Perdew and Wang[47] and ultrasoft pseudopotentials[48] with a cutoff energy of 250 eV. Total-energy calculations were performed on periodic supercells of NaAlH$_4$ {Na$_3$AlH$_6$} that contained 768 {960} atoms in the defect-free phases. Temperature-dependent vibrational contributions to the free energy[49] were calculated for all pure and defected structures and included where relevant in determining $\Delta G_i(\text{def})$ and the chemical potentials. In addition, the temperature- and pressure-dependent contributions to the gas-phase free energy of H$_2$ were included in determining the chemical potential of hydrogen. The diffusivities of defects were calculated using kinetic Monte Carlo simulations that were parameterized by DFT calculations. These simulations were performed at a finite number of temperatures over a range relevant to Reaction (1); for a detailed discussion of these methods, see Ref. 41.

Table 1 Temperature dependence of reaction rates in the morphologies shown in Figure 1, given as powers of $(D\Delta C)^n$. Ranges indicate values of n that change over time due to changing diffusion distances, with the left (right) values corresponding to early (late) reaction times.

Morphology	Dehydrogenation	Rehydrogenation
Linear ($d = 1$)		
Figure 1(a)	$n = 1/2$	$1 \geq n \geq 1/2$
Figure 1(b)	$1 \geq n \geq 1/2$	$n = 1/2$
Lamellar ($d = 2$)		
Figure 1(c)	$n = 1$	$n = 1$
Core-shell ($d = 3$)		
Figure 1(d)	$n = 3/2$	$1 \leq n \leq 3/2$
Figure 1(e)	$1/2 \leq n \leq 3/2$	$3/2 \geq n \geq 1/2$

Table 2 Native defects considered in $NaAlH_4$ and Na_3AlH_6

defect	$NaAlH_4$	Na_3AlH_6
$[Al]^{3-}$	•	•
$[AlH]^{2-}$	•	•
$[AlH_2]^{-}$	•	•
$[AlH_3]$	•	•
$[AlH_4]^{+}$	•	•
$[AlH_5]^{2+}$		•
$[AlH_6]^{3+}$		•
$[Na]^{-}$	•	•
$[NaH]$	•	•
$[H]^{+}$	•	•
$[H]^{-}$	•	•
$^{i}H^{+}$	•	•
$^{i}H^{-}$	•	•

2.4 Summary of reaction rates and connection to experiment

Our analytic results for the exponent of $(D\Delta C)^n$ in the temperature dependence of the reaction rate are summarized in Table 1 (derivations can be found in the appendix). The key finding is that n depends on the reaction morphology and several morphologies exhibit values of n that vary with time due to changing diffusion distances as the reactants and products shrink or grow. It is, however, unclear at this point which morphology should be used to describe the mass transport rate in Reaction (1).

Sandrock *et. al.* have measured the rates of hydrogen release and absorption from Ti-catalyzed $NaAlH_4$ as functions of time, which are shown in Figs. 1 and 2 of Ref. 7. Their measurements indicate that the hydrogen release and absorption rate remains constant during most of the total reaction time, which is consistent only with the two-dimensional lamellar morphology in Figure 1(c), for which the reaction rate is given by Eq. (21) [the reaction rates for one- and three-dimensional morphologies are expected to change over time by Eqs. (17), (20), (26), and (28)]. We therefore calculate all following defect fluxes assuming that $J \propto D\Delta C$ as given by Eq. (21) and take this value to be independent of time.

Using the calculated fluxes, the activation energy, E_{act} can be extracted by fitting the Arrhenius equation to this data:

$$J = J_0 e^{-E_{act}/RT}, \qquad (12)$$

where J_0 is the Arrhenius pre-factor, R is the gas constant and T is the temperature. When evaluating the flux given in Eq. (21), we define the concentration gradient as $\nabla C_i = \Delta C_i / \Delta l$ where ΔC_i is the difference in concentrations of defects between two interfaces that are separated by a distance Δl. The choice of Δl is inconsequential when comparing to experimental activation energies since in the 2D lamellar morphology

it is a constant and can be incorporated in the temperature-independent pre-factor of the Arrhenius equation. Fluxes of various defects are compared with the arbitrary choice of Δl = 1 μm since this is consistent with the particle size of ball-milled samples of $NaAlH_4$.[50]

3 Results

The defects that have been studied in $NaAlH_4$ and Na_3AlH_6 (see Figure 2) are listed in Table 2. These defects are identical to those discussed in Ref. 40. The naming convention of native vacancies is such that bracketed $[X]^q$ represents a vacancy of X in charge state q. Interstitial defects are labeled with a superscript "i" so that $^{i}X^q$ is an interstitial defect of type X in charge state q. The following subsections cover the concentration gradients and fluxes of defects in $NaAlH_4$ and in Na_3AlH_6. We also include a brief discussion on Reaction (2) and the rate of mass transport through Na_3AlH_6 for this case.

3.1 Concentration Gradients and Fluxes in $NaAlH_4$

We begin by examining concentration gradients across $NaAlH_4$, shown on Arrhenius plots in Figures 3(a) and (b). Since these plots show absolute values of the gradients ($\Delta C / \Delta l$ with Δl = 1 μm), the inset morphology (and in all other figures showing a concentration gradient or flux) gives the net direction of diffusion of the defects. For example, in the plot shown in Figure 3(a), these defects migrate to the Al interface at low temperatures and to the Na_3AlH_6 interface at high temperatures, in accord with the metal mass flux required for the rehydrogenation and dehydrogenation reactions, respectively. In the plot shown in Figure 3(b), these directions are reversed since Na-site defects move oppositely to Al-site defects at any
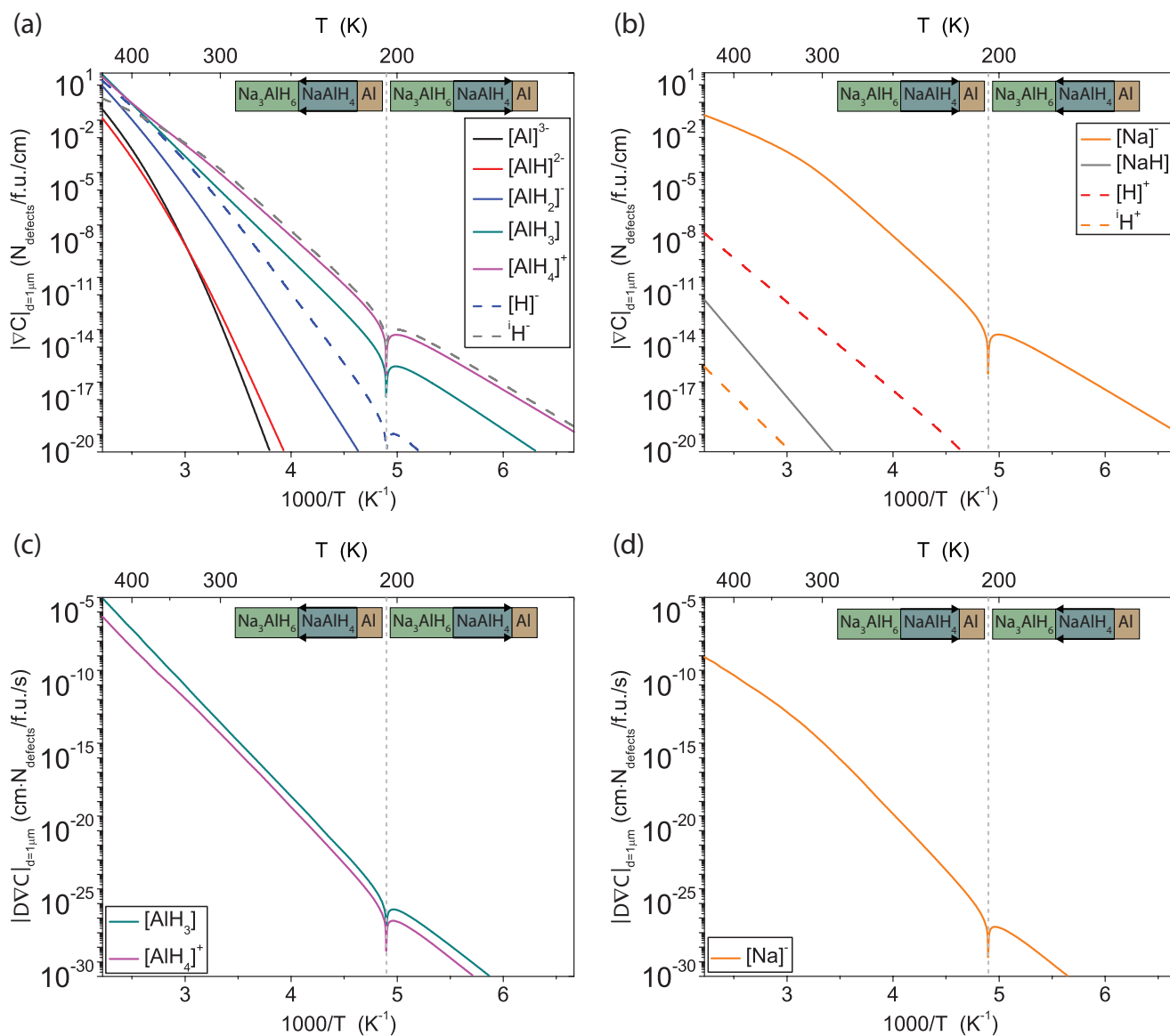
Fig. 3 Concentration gradients and fluxes of defects across a 1 μm region of NaAlH$_4$.
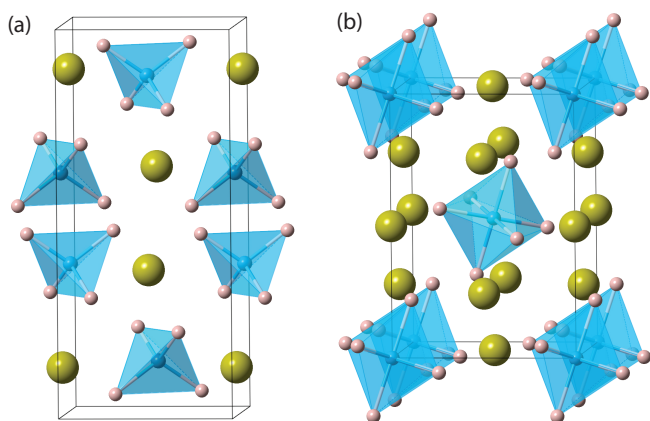
Fig. 2 Conventional cells of NaAlH$_4$ (a) and Na$_3$AlH$_6$ (b) with Al ions in blue, Na ions in yellow, and H ions in pink.

given temperature.

We find that the NaAlH$_4$ defects with the largest concentration gradients are positively charged AlH$_4$ vacancies, neutral AlH$_3$ vacancies, and three negatively charged defects: Na vacancies, H vacancies, and H interstitials. Since the chemical potential of hydrogen is the same at all interfaces under the assumed equilibrium conditions with H$_2$ gas, the concentration gradients of charged H vacancies and H interstitials are entirely due to the Fermi level gradient that is formed by local charge neutrality conditions at each interface. At low temperatures, the concentration gradients of negatively charged H interstitials, negatively charged Na vacancies, and positively charged AlH$_4$ vacancies are the largest. At higher temperatures (approximately 350 K and above), the concentration gradient of Na vacancies becomes less significant and that of negatively charged H vacancies is larger.

Multiplying the concentration gradients of defects in Figures 3(a) and (b) by their spatially-averaged diffusivities,[41] the resulting fluxes through NaAlH$_4$ are shown in Figures 3(c) and (d). The largest flux of metal-site defects is identified as neutral AlH$_3$ vacancies followed by positively charged AlH$_4$ vacancies and negatively charged Na vacancies. This is in agreement with previous theoretical studies[38] and experimental work in which mobile Al$_x$H$_y$ species have been identified in NaAlH$_4$.[51] Fitting the Arrhenius equation to the high-temperature (dehydrogenation) region, the activation energies for $J \propto D\nabla C$ are 146 kJ/mol for AlH$_3$ vacancies, 143 kJ/mol for AlH$_4$ vacancies, and 135 kJ/mol for Na vacancies. All of these are significantly above the experimental activation energies for the reaction (118 kJ/mol in pure samples and 73-80 kJ/mol in Ti-doped samples[6]), ruling out the possibility that dehydrogenation occurs in the 2D or 3D morphologies shown in Figures 1(c)-(e) (see also Table 1). The calculated activation energy values are compatible with the morphology shown in

Figure 1(b) which predicts a $(D\nabla C)^n$ temperature dependence with $n = \frac{1}{2}$, but such a scenario is difficult to reconcile with the nearly constant dehydrogenation rate observed by Sandrock *et al.*[7] in Ti-catalyzed samples. Therefore, we conclude that the fastest mode of mass transport in these samples occurs via some other process than bulk diffusion through NaAlH$_4$.

The activation energy for rehydrogenation was obtained by increasing the pressure of H$_2$ gas to 100 bar. A fit of the Arrhenius equation to these results shows that the activation energy for the defect flux under rehydrogenation conditions is approximately 110 kJ/mol for AlH$_3$, AlH$_4$, and Na vacancies. Again, these are well-above the experimental activation energy for the rehydrogenation reaction in Ti-doped samples (62 kJ/mol[14]) so that these defects cannot be involved in the rate-limiting process in any of the 2D or 3D morphologies in Figures 1(c)-(e), but they cannot be ruled out if one assumes the 1D morphology shown in Figure 1(b), for which under rehydrogenation conditions one obtains $n > 1/2$ (see Table 1). However, it will be shown in the following section that rates of mass transport are higher for defects in Na$_3$AlH$_6$ under both de- and rehydrogenation conditions so that transport through NaAlH$_4$ should not be rate-limiting.

3.2 Concentration Gradients and Fluxes in Na$_3$AlH$_6$

Concentration gradients across Na$_3$AlH$_6$ are shown in Figure 4(a). The only metal defect that has an appreciable concentration gradient is an Na vacancy, the charge of which is balanced by H vacancies. All other calculated metal defect concentration gradients are at least two orders of magnitude lower with neutral NaH vacancies forming in the largest concentration gradients after Na vacancies.

Using the spatially-averaged diffusivity of Na vacancies in Na$_3$AlH$_6$[41] and the concentration gradient given in Figure 4(a), the flux of this defect is shown in Figure 4(b). The charge of the Na vacancies is balanced by that of hydrogen vacancies; the hydrogen vacancy flux has been shown to be larger than the Na vacancy flux so the latter type is the rate-limiting of the two.[41] Comparing the flux of Na vacancies through Na$_3$AlH$_6$ [Figure 4(b)] to the flux of metal defects through NaAlH$_4$ [Figures 3(a) and (b)], it is clear that mass transport is dominated by defects in Na$_3$AlH$_6$ since the flux in this phase is higher by orders of magnitude at a given temperature and distance between interfaces. We conclude that a product phase of Reaction (1) is the medium through which the fastest mode of long-range mass transport occurs.

Fitting of the Arrhenius equation to $J \propto D\nabla C$ for Na vacancies in Na$_3$AlH$_6$ yields an activation energy of 70 kJ/mol in the high-temperature (dehydrogenation) region, which agrees well with the experimental activation energy for Reaction (1) when doped with Ti (73-80 kJ/mol) if one assumes a 2D reaction morphology shown in Figure 1(c) for which $n = 1$ (see
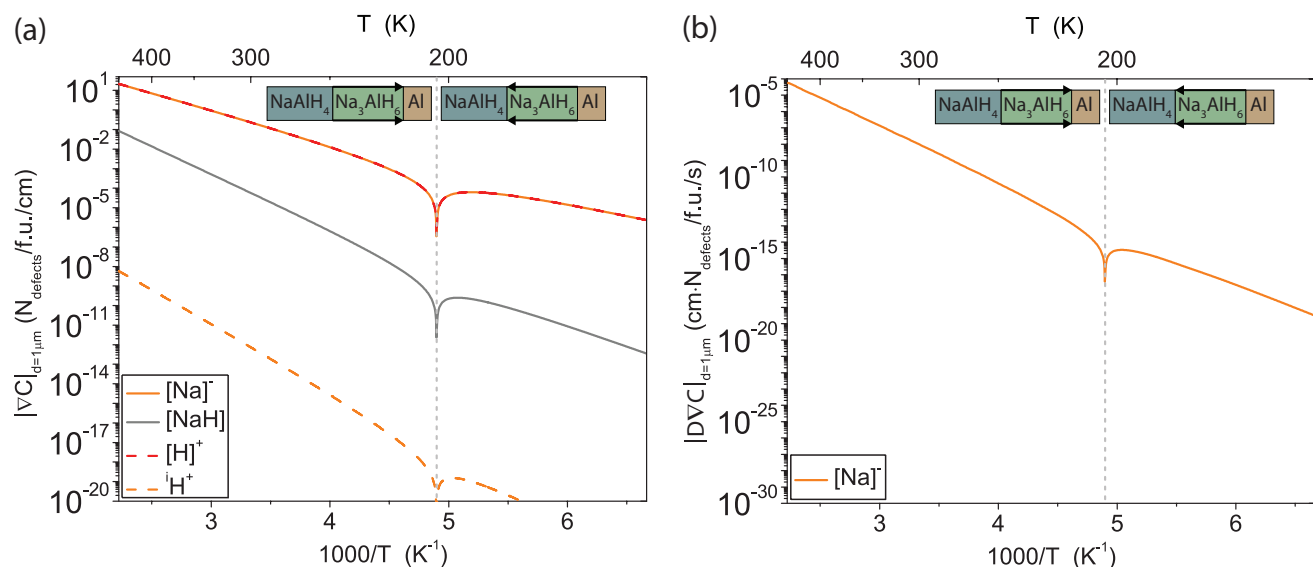
Fig. 4 Concentration gradients and fluxes of defects across a 1 μm region of Na_3AlH_6.

Table 1). Since the 2D morphology is also consistent with the constant hydrogen release rates observed experimentally,[7] we therefore identify the flux of charged Na vacancies through Na_3AlH_6 as the rate-limiting process in the dehydrogenation of Ti-doped $NaAlH_4$.

The proposed model also predicts the existence of kinetic isotope effect (KIE) in deuterated samples. Experimental results have shown that the ratio of activation energies in hydrogenated and deuterated $NaAlH_4$ ($NaAlD_4$) is 0.93 under hydrogen (deuterium) release conditions when the system is doped with Ti.[9] Deuterium mass affects the calculated frequencies of the vibrational modes and hence the vibrational energies (including zero-point effects) and entropies of all defects and coexisting phases. The calculations involving Na vacancies in Na_3AlH_6 were repeated with the mass of deuterium exchanged for the mass of hydrogen. The vibrational properties of all pure and defected structures were recalculated and the concentration gradients of defects were obtained following Eqs. (7)-(9). In addition, the vibrational modes of the deuterated ground and transition state structures of an Na vacancy in Na_3AlH_6 were used as input for a separate KMC simulation following the same procedure as in Ref. 41. The activation energies were obtained for hydrogenated and deuterated systems from fits of the Arrhenius equation to the flux of Na vacancies in Na_3AlH_6 and Na_3AlD_6. The ratio of these activation energies was found to be 0.97, in reasonable agreement with the experimental result of 0.93, and significantly different from the value of approximately 0.71 expected for hydrogen bond-breaking or diffusion.[9]

With the H_2 pressure increased to 100 bar, the calculated ac-

tivation energy for the flux of Na vacancies through Na_3AlH_6 under rehydrogenation conditions is 50 kJ/mol. This is lower than the experimentally-measured activation for rehydrogenation of Ti-doped $NaAlH_4$ (62 kJ/mol was obtained in Ref. 14) but in line with the approximately 10 kJ/(mol H_2) underestimation of formation enthalpies that is typical of DFT results relative to experimental reaction enthalpies for $NaAlH_4$ [40] (enthalpy errors will manifest in the calculated chemical potentials and hence in the formation energies of defects and their concentration gradients). Hence, we propose that Na vacancy diffusion through Na_3AlH_6 is also the rate-limiting step in dehydrogenation of Ti-catalyzed samples. We are not aware of any experimentally-measured activation energies for the rehydrogenation of $NaAlH_4$ in uncatalyzed reactions, but this must be at least equal to the activation energy of Ti-catalyzed rehydrogenation. It is likely that some other process, such as nucleation or H_2 dissociation, represents the rate-limiting step during rehydrogenation of pure $NaAlH_4$. Indeed, recent computational study of H_2 dissociation on pure and Ti-doped Al surface by Wang *et al.*[52] comes to such a conclusion.

3.3 Defect Flux Through Na_3AlH_6 During Reaction (2)

It is straightforward at this point to examine defect fluxes in Na_3AlH_6 under the conditions of Reaction (2). For reasons already discussed in Ref. 40, the flux of Na through Al can be ignored. Similarly, the flux of Al through NaH will be insignificant due to the immiscibility of Al and NaH. Having already calculated $\Delta G_i(\text{def})$ in Eq. (8) for each defect in Na_3AlH_6, only the chemical potentials of elemental species and electrons must be determined. In this case, the chemical

potentials are fixed by interfaces of Na_3AlH_6 with either Al or NaH. Again we find that the fluxes of negatively charged Na vacancies and positively charged hydrogen vacancies dominate all other defect fluxes in this phase. We find that the activation energies for the flux $D\nabla C$ under de- and rehydrogenation conditions are 73 and 52 kJ/mol, respectively. Since the calculated activation energy for dehydrogenation (73 kJ/mol) is so far below measured values in pure (121 kJ/mol[6]) or Ti-doped (97 kJ/mol[6]) systems, it is unlikely that mass transport represents the rate-limiting process in either. However, the calculated and measured activation energies for rehydrogenation agree well (52 and 56[14] kJ/mol, respectively) and with this we conclude that mass transport could be a kinetic bottleneck during rehydrogenation of Na_3AlH_6 from NaH and Al.

4　Discussion and Conclusions

In this paper, we have formulated a mass transport model for solid-state decomposition reactions involving multiple product phases and gaseous species. This model uses local equilibrium assumptions at the solid-solid interphase boundaries to determine local defect concentrations and concentration gradients driving metal fluxes during decomposition. Charge compensation conditions are also imposed locally at each interface, coupling the concentrations of positively and negatively charged defects via the local Fermi level. As a result, large fluxes are found also for charged hydrogen vacancies and interstitials, which are being driven by Fermi level gradients. A crucial advantage of the model is that all the required quantities - defect formation energies, total energies of phases, and diffusivities of defects - can be obtained from first-principles DFT calculations, allowing for a quantitative comparison with the experimental data on activation energies.

The results of this work show that the mass transport of metal species during Reaction (1) is dominated by the flux of Na vacancies in Na_3AlH_6, a product phase of this reaction. We have shown strong evidence that this represents the rate-limiting process in Ti-catalyzed reactions where the calculated activation energy for this process (70 kJ/mol) agrees well with the experimentally determined activation energy for the overall reaction (73-80 kJ/mol[6]). Under rehydrogenation conditions, mass transport is also dominated by the flux of Na vacancies in Na_3AlH_6. The calculated activation energy for this process is 50 kJ/mol, which is again comparable to the experimental activation energy for rehydrogenation of Ti-doped $NaAlH_4$ (62 kJ/mol[14]).

It was shown in Ref. 42 that equilibrium concentrations of charged and neutral Ti defects in bulk $NaAlH_4$ and Na_3AlH_6 are many orders of magnitude lower than native defect concentrations and cannot have an effect on the native defect fluxes. Even in highly non-equilibrium concentrations approaching 10^{-4} defects/f.u., the effects of bulk Ti are negligible at nor-

mal reaction conditions. Therefore, the defect fluxes and activation energies shown in this paper hold true for either pure or Ti-doped samples. In other words, Ti does not catalyze bulk defect diffusion. Instead, the rate-limiting step of Reaction (1) in undoped samples is some other process such as nucleation or H_2 combination/dissociation. It is this other process (which we are not able to identify from the present calculations) that must be catalyzed by Ti. However, we have shown that bulk defect diffusion becomes the rate-limiting process once Ti has been added. Therefore, further catalysis of Reaction (1) would necessarily involve lowering the activation energies for the formation and migration of bulk defects.

As with $NaAlH_4$, other complex metal hydrides generally suffer from slow (de)hydrogenation rates. Since mass transport has been suggested as a possible rate-limiting process during these reactions, hydrogen storage materials can be designed to maximize the reaction rates by choosing compounds that are known to be fast ionic conductors and can also form hydrogenated phases. Of course, other processes may limit the rate of reaction, but if metal segregation occurs, this serves as at least one general guideline for the design of hydrogen storage materials with fast reaction rates.

The theory of mass transport proposed here is only the first step towards constructing a comprehensive atomistic framework of the kinetics of solid state decomposition reactions. For future work, detailed experimental studies and large-scale computer simulations of nucleation and growth are needed to understand the morphology selection mechanisms and their dependence on the material parameters and reaction conditions. A complete theory of reaction kinetics should also consider the effects of particle size distribution on the measured hydrogen release rates. Models of interfacial reaction kinetics describing the cleavage of interatomic bonds and interconversion of complex hydride phases are needed to quantitatively describe the kinetics of defect generation and equilibration and evaluate the range of validity of the local equilibrium assumption adopted here. For instance, in very small particles diffusion times may drop below the interfacial reaction rates due to decreasing particle size and increasing importance of fast surface diffusion pathways, leading to decrease in the apparent activation energies and faster reaction kinetics.[11]

5　Appendix

In this appendix are solutions to Eq. 5 under the three morphologies (1, 2, and 3-dimensional) discussed in the section titled Reaction Morphologies. These solutions give the dependence of the flux on $D\nabla C$ that is summarized in Table 1.

5.1 One-dimensional linear morphology

Consider dehydrogenation in one-dimensional morphologies, such as shown in Figures 1(a) and (b). Let $W(t)$ denote the thickness of the middle region through which the mass transport occurs at time t. We solve Eq. (6) subject to the following moving boundary conditions: $C|_{x=0} = C^L$ and $C|_{x=W(t)} = C^R$. Introducing the concentration difference $\Delta C = C^L - C^R$, the solution to the boundary value problem can be written as:

$$C(x,t) = C^L - \frac{\Delta C}{W(t)} x. \tag{13}$$

The flux is given by

$$J(t) = -D\frac{\partial C}{\partial x} = \frac{D\Delta C}{W(t)}, \tag{14}$$

and the rate of movement of the boundaries is directly proportional to the flux:

$$\frac{dW}{dt} = JS\delta a = J\delta V = \frac{D\Delta C\delta V}{W}, \tag{15}$$

where S is the cross-sectional area and δa is the "thickness" added (or subtracted) by absorbing one unit of defect at the right interface; the product of these gives the "volume" of the defect, δV, which can be positive or negative, depending on the direction of interface movement. We need to distinguish between two cases when solving Eq. (15): case 1 being diffusion through a product phase of the reaction (Na_3AlH_6) and case 2 through a reactant ($NaAlH_4$).

Case 1: Assume that the middle phase is a reaction product [Na_3AlH_6, see Figure 1(a)], which was nucleated at the start of the dehydrogenation reaction, so that the initial width is $W(0) = 0$. Integrating Eq. (15), the phase grows with a width at time t, $W(t)$, equal to

$$W(t) = \sqrt{2D\Delta C|\delta V|t}. \tag{16}$$

Correspondingly, for the flux in Eq. (14) we obtain

$$J(t) = \sqrt{\frac{D\Delta C}{2|\delta V|t}}. \tag{17}$$

The reaction rate is proportional to the flux multiplied by the total interfacial area; the latter does not change with time, while the former has an inverse square-root dependence due to the lengthening of the diffusion path with increasing width of the product phase. In this case, the temperature dependence of the reaction rate enters through $\sqrt{D\Delta C}$, not $D\Delta C$ as would be expected assuming a constant W.

The time to complete the reaction is equal to

$$\tau_c = \frac{W_0^2}{2D\Delta C|\delta V|}. \tag{18}$$

Assuming $W_0 = 1 \ \mu m$ and $T = 400$ K, we can use the calculated values of $D = 10^{-4}$ cm^2/s[41] and $\Delta C = 10^{-4}$ defects/f.u.[40], along with $|\delta V| \approx 1$ f.u./defect, to estimate a completion time on the order of seconds, which is faster than the observed dehydrogenation times of minutes and hours, but quite reasonable given the approximations that are involved in this estimate.

Case 2: If the middle phase is the reactant [$NaAlH_4$, see Figure 1(b)], it shrinks from the initial width $W(0) = W_0$ to zero at the end of the dehydrogenation reaction. The defect volume δV in Eq. (15) is negative, and after integrating Eq. (15), the width is equal to

$$W(t) = \sqrt{W_0^2 - 2D\Delta C|\delta V|t}, \tag{19}$$

while the flux is given by

$$J(t) = \frac{D\Delta C}{\sqrt{W_0^2 - 2D\Delta C|\delta V|t}}. \tag{20}$$

The flux and the reaction rate increase with time due to the shortening of the diffusion path. The temperature dependence of the reaction rate is given by $D\Delta C$ at early times when the time factor in the denominator can be neglected in comparison with the initial width W_0. However, at late times (near the completion time τ_c) the apparent temperature dependence of the reaction again approaches $\sqrt{D\Delta C}$, while the reaction rate diverges as $(\tau_c - t)^{-\frac{1}{2}}$.

5.2 Two-dimensional lamellar morphology

For the lamellar morphology shown in Figure 1(c), one needs to solve the stationary diffusion equation in two dimensions with moving boundary conditions that preserve the similarity of the interface shapes, which can only be accomplished numerically. Here, we limit ourselves to a qualitative discussion of the expected results. As discussed previously, the shape of the Al lamellae depends on the relative magnitude of the diffusion rates in the two hydrides, $D_{[AlH_x]}$ and $D_{[Na]}$. In the limiting case when one of the diffusion mechanisms dominates over the other, the total reaction rate Φ is proportional to the flux,

$$\Phi \propto J \propto \frac{D\Delta C}{\Delta l} = \text{const.}, \tag{21}$$

where Δl is the lamellar spacing, which may depend on the reaction conditions, such as hydrogen partial pressure and temperature, but otherwise stays constant during the reaction. The temperature dependence of the reaction rate is expected to vary as $D\Delta C$, even though additional corrections due to the T-dependence of the lamellar spacing cannot be excluded. The velocity of the reaction front stays constant, and time to completion will be inversely proportional to the flux:

$$\tau_c \propto \frac{R_0\Delta l}{D\Delta C}, \tag{22}$$

where R_0 is the initial radius of the hydride particle.

5.3 Three-dimensional core-shell morphologies

The morphologies shown in Figures 1(d) and (e) permit analytic solutions if one assumes spherical symmetry. We consider the case of dehydrogenation according to Figure 1(d) and denote by $R(t)$ the radius of the Al (core) particle and by $W(t)$ the width of the envelope shell around it. The volume ratio of the Al particle and the enclosing shell of Na_3AlH_6 stays constant during the reaction: $V_{shell}(t) = \alpha' V_{core}(t)$ where α' is determined by the densities and mole fractions of the product phases in Reaction (1). Expanding the previous equation and dropping the common prefactors of $4\pi/3$, $[R(t) + W(t)]^3 - R(t)^3 = \alpha' R(t)^3$, which, when solved for $W(t)$, has only one real solution: $W(t) = \alpha R(t)$ where $\alpha = -1 + (1 + \alpha')^{1/3}$ is again a constant.

The stationary diffusion equation [Eq. (6)] in spherical coordinates reduces to $\frac{\partial^2 C}{\partial r^2} + \frac{2}{r}\frac{\partial C}{\partial r} = 0$, and the boundary conditions are $C|_{r=R(t)} = C^1$ and $C|_{r=(1+\alpha)R(t)} = C^2$, where C^1 and C^2 are the equilibrium defect concentrations at the two interfaces surrounding the Na_3AlH_6 shell. Introducing the concentration difference $\Delta C = C^1 - C^2$, this boundary value problem can be easily solved:

$$C(r,t) = C^1 - \Delta C \frac{(1+\alpha)[r - R(t)]}{\alpha r}. \tag{23}$$

The corresponding flux is given by

$$J(r,t) = -D\frac{\partial C}{\partial r} = \frac{D\Delta C(1+\alpha)R}{\alpha r^2}, \tag{24}$$

and the time evolution of the growing Al particle radius can be found by solving $dR/dt = J(R,t)\delta V$ subject to $R(0) = 0$. This gives

$$R(t) = \sqrt{\frac{2D\Delta C\delta V(1+\alpha)t}{\alpha}}, \tag{25}$$

and the reaction rate is proportional to the total flux of defects reaching the Al core:

$$\Phi = 4\pi r^2 J(r,t)\big|_{r=R(t)} = 4\pi\sqrt{\frac{2(D\Delta C)^3(1+\alpha)^3 t}{\alpha^3}}. \tag{26}$$

At the completion of the reaction, the sum of the Al core radius and the thickness of the Na_3AlH_6 shell equals the total particle size R_0, hence $R(\tau_c) = R_0/(1 + \alpha)$. Time to completion is analogous to the expression for the 1D case:

$$\tau_c = \frac{\alpha R_0^2}{2D\Delta C|\delta V|(1+\alpha)^3}. \tag{27}$$

Similar expressions can be derived for the rehydrogenation reaction which proceeds by reversing the vacancy flux in Figure 1(d). Following the steps above and modifying the initial

condition for $R(t)$ to $R(0) = R_0/(1 + \alpha)$, we find that the reaction rate can be written as

$$\Phi = 4\pi D\Delta C R_0 \sqrt{\frac{\tau_c - t}{\alpha\tau_c}}, \tag{28}$$

where the completion time τ_c is given by Eq. (27). At short times, the reaction rate is approximately constant and given by $\Phi = 4\pi D\Delta C R_0/\sqrt{\alpha}$, while near completion it becomes proportional to $(D\Delta C)^{\frac{3}{2}}\sqrt{\tau_c - t}$.

Solutions for the morphology shown in Figure 1(e) cannot be found analytically because in general the relation between the radius of the Al core and the surrounding $NaAlH_4$ shell is nonlinear. However, asymptotic solutions can be found in the limit of both early and late stages of the reaction. Here we omit these rather cumbersome derivations and only state the main results. For dehydrogenation, the reaction rate behaves as $\Phi \propto \sqrt{D\Delta C/t}$ when $t \to 0$ and $\Phi \propto (D\Delta C)^{\frac{3}{2}}\sqrt{\tau_c - t}$ as $t \to \tau_c$ (note, however, that an explicit formula for τ_c could not be found). For rehydrogenation, the flux of AlH_x vacancies and the initial conditions are reversed, i.e. $R(0) = 0$ and $R(\tau_c) = R_0/(1 + \alpha)$. The corresponding reaction rates are given by $\Phi \propto (D\Delta C)^{\frac{3}{2}}\sqrt{t}$ and $\Phi \propto \sqrt{D\Delta C/(\tau_c - t)}$ for $t \to 0$ and $t \to \tau_c$, respectively.

References

1 S. Satyapal, J. Petrovic, C. Read, G. Thomas and G. Ordaz, *Catal. Today*, 2007, **120**, 246–256.

2 S. McWhorter, C. Read, G. Ordaz and N. Stetson, *Curr. Opin. Solid State and Mater. Sci.*, 2011, **15**, 29 – 38.

3 B. Bogdanovic and M. Schwickardi, *J. Alloy. Compd.*, 1997, **253-254**, 1 – 9.

4 K. Gross, S. Guthrie, S. Takara and G. Thomas, *J. Alloy. Compd.*, 2000, **297**, 270–281.

5 C. Jensen and K. Gross, *Appl. Phys. A-Mater.*, 2001, **72**, 213–219.

6 K. Gross, G. Thomas and C. Jensen, *J. Alloy. Compd.*, 2002, **330**, 683–690.

7 G. Sandrock, K. Gross and G. Thomas, *J. Alloy. Compd.*, 2002, **339**, 299–308.

8 O. Kircher and M. Fichtner, *J. Alloy. Compd.*, 2005, **404**, 339–342.

9 W. Lohstroh and M. Fichtner, *Phys. Rev. B*, 2007, **75**, 184106.

10 A. Borgschulte, A. Zuettel, P. Hug, G. Barkhordarian, N. Eigen, M. Dornheim, R. Bormann and A. J. Ramirez-Cuesta, *Phys. Chem. Chem. Phys.*, 2008, **10**, 4045–4055.

11 C. P. Balde, B. P. C. Hereijgers, J. H. Bitter and K. P. D. Jong, *J. Am. Chem. Soc.*, 2008, **130**, 6761–6765.

12 E. C. Ashby and P. Kobetz, *Inorg. Chem.*, 1966, **5**, 1615–1617.

13 T. Dymova and S. Bakum, *Russ. J. Inorg. Chem.*, 1969, **14**, 1683.

14 W. Luo and K. J. Gross, *J. Alloy. Compd.*, 2004, **385**, 224 – 231.

15 S. Alapati, J. Johnson and D. Sholl, *J. Phys. Chem. B*, 2006, **110**, 8769–8776.

16 A. R. Akbarzadeh, V. Ozolins and C. Wolverton, *Adv. Mater.*, 2007, **19**, 3233–3239.

17 C. Wolverton and V. Ozolins, *Phys. Rev. B*, 2007, **75**, 064101.

18 D. J. Siegel, C. Wolverton and V. Ozolins, *Phys. Rev. B*, 2007, **75**, 014101.

19 D. J. Siegel, C. Wolverton and V. Ozolins, *Phys. Rev. B*, 2007, **76**, 134102.

20 S. V. Alapati, J. K. Johnson and D. S. Sholl, *J. Phys. Chem. C*, 2007, **111**, 1584–1591.

21 S. V. Alapati, J. K. Johnson and D. S. Sholl, *Phys. Chem. Chem. Phys.*, 2007, **9**, 1438–1452.

22 C. Wolverton, D. J. Siegel, A. R. Akbarzadeh and V. Ozolins, *J. Phys.-Condens. Mat.*, 2008, **20**, 064228.

23 V. Ozolins, E. H. Majzoub and C. Wolverton, *Phys. Rev. Lett.*, 2008, **100**, 135501.

24 Z. Xiong, C. K. Yong, G. Wu, P. Chen, W. Shaw, A. Karkamkar, T. Autrey, M. O. Jones, S. R. Johnson, P. P. Edwards and W. I. F. David, *Nat. Mater.*, 2008, **7**, 138–141.

25 A. Sudik, J. Yang, D. Halliday and C. Wolverton, *J. Phys. Chem. C*, 2008, **112**, 4384–4390.

26 V. Ozolins, E. H. Majzoub and C. Wolverton, *J. Am. Chem. Soc.*, 2009, **131**, 230–237.

27 K. J. Michel, A. R. Akbarzadeh and V. Ozolins, *J. Phys. Chem. C*, 2009, **113**, 14551–14558.

28 K. C. Kim and D. S. Sholl, *J. Phys. Chem. C*, 2010, **114**, 678–686.

29 O. Kircher and M. Fichtner, *J. Appl. Phys.*, 2004, **95**, 7748–7753.

30 C. Araujo, R. Ahuja, J. Guillen and P. Jena, *Appl. Phys. Lett.*, 2005, **86**, 251913.

31 S. Chaudhuri and J. Muckerman, *J. Phys. Chem. B*, 2005, **109**, 6952–6957.

32 J. Iniguez and T. Yildirim, *Appl. Phys. Lett.*, 2005, **86**, 103109.

33 O. Lovvik and S. Opalka, *Phys. Rev. B*, 2005, **71**, 054103.

34 O. Lovvik and S. Opalka, *Appl. Phys. Lett.*, 2006, **88**, 161917.

35 A. Blomqvist, C. M. Araujo, P. Jena and R. Ahuja, *Appl. Phys. Lett.*, 2007, **90**, 141904.

36 A. Peles and C. G. V. D. Walle, *Phys. Rev. B*, 2007, **76**, 214101.

37 Z. Lodziana, A. Zuettel and P. Zielinski, *J. Phys.-Condens. Mat.*, 2008, **20**, 465210.

38 H. Gunaydin, K. N. Houk and V. Ozoliņš, *PNAS*, 2008, **105**, 3673–3677.

39 G. B. Wilson-Short, A. Janotti, K. Hoang, A. Peles and C. G. Van de Walle, *Phys. Rev. B*, 2009, **80**, 224102.

40 K. Michel and V. Ozoliņš, *J. Phys. Chem. C*, 2011, **115**, 21443–21453.

41 K. Michel and V. Ozoliņš, *J. Phys. Chem. C*, 2011, **115**, 21465–21472.

42 K. Michel and V. Ozoliņš, *J. Phys. Chem. C*, 2011, **115**, 21454–21464.

43 K. Sakaki, Y. Nakamura, E. Akiba, M. T. Kuba and C. M. Jensen, *J. Phys. Chem. C*, 2010, **114**, 6869–6873.

44 W. W. Mullins and R. F. Sekerka, *J. Appl. Phys.*, 1964, **35**, 444–451.

45 R. W. Balluffi, S. Allen and W. C. Carter, *Kinetics of Materials*, Wiley, 2005.

46 G. Kresse and J. Furthmuller, *Phys. Rev. B*, 1996, **54**, 11169–11186.

47 J. P. Perdew, J. A. Chevary, S. H. Vosko, K. A. Jackson, M. R. Pederson, D. J. Singh and C. Fiolhais, *Phys. Rev. B*, 1992, **46**, 6671–6687.

48 D. Vanderbilt, *Phys. Rev. B*, 1990, **41**, 7892–7895.

49 C. Wolverton, V. Ozolins and M. Asta, *Phys. Rev. B*, 2004, **69**, 144109.

50 M. Balogh, G. Tibbetts, F. Pinkerton, G. Meisner and C. Olk, *J. Alloy. Compd.*, 2003, **350**, 136–144.

51 T. M. Ivancic, S.-J. Hwang, R. C. Bowman, D. S. Birkmire, C. M. Jensen, T. J. Udovic and M. S. Conradi, *J. Phys. Chem. Lett.*, 2010, **1**, 2412–2416.

52 Y. Wang, F. Zhang, R. Stumpf, P. Lin and M. Y. Chou, *Phys. Rev. B*, 2011, **83**, year.